UNIVERSITY OF AMSTERDAM

MSc Physics and Astronomy
Track: Astronomy & Astrophysics

Master Thesis

Investigating High Mass X-Ray Binaries With GAIA DR3

Subtitle of Thesis
Can use two lines

by

Karan Kumar
14906619(UVA)

January 31, 2025
60 ECTS
02-09-2024 - End date

Supervisors:
Lex Kaper
Daily Supervisor

Examiners
Alex De Koter

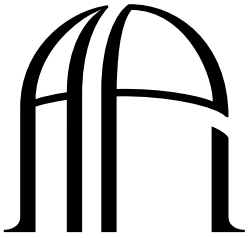

ANTON PANNEKOEK
INSTITUTE

Contents

List of Figures

List of Tables

Chapter 1

Introduction

High mass X-ray binaries (HMXBs) consist of a massive star O-type or B-type known as the companion orbiting a compact X-ray source. Typically, the compact object is a neutron star or black hole. The X-rays are produced via accretion from the massive companion either by stellar wind mass loss or by Roche-Lobe overflow van den Heuvel et al. (2000). Runaways form when the binary system is ejected out of the galactic plane or if the system has a high peculiar velocity. ($\geq$ 20-30 km/s) Although this velocity isn't constrained to this limit Carretero-Castrillo et al. (2023). Since their prediction by Blaauw (1961) HMXBs have been observed through various space telescopes, the very first with *Hipparcos* Chevalier & Ilovaisky (1998); Moffat et al. (1998) and *Gaia* Carretero-Castrillo et al. (2023); Maíz Apellániz et al. (2018). My project is to use *Gaia* DR3 to search for HMXB runaways, measure their space velocity, and reconstruct the evolutionary history of the binary system. Gaia Collaboration et al. (2023)

1. stars typically travel 100 PC over their lifetime (10^7) and we see stars beyond that (that is 10km/s)

1.1 GAIA Space Telescope by ESA

The *Gaia* space mission run by the European Space Agency provides astrometry of stars in the galaxy with great precision; it measures the position, proper motions and brightness of stars in the galaxy and is the successor to the *Hipparcos* space mission. *Hipparcos*, which ran from 1989 to 1993, measured the parallax (ω), right ascension (α), declination (δ), Proper Motion in Right Ascension (μ_α), and Proper Motion in declination (μ_δ). This is known as the equatorial coordinate system, which maps the coordinates onto a projection of the celestial frame. In literature these

coordinates make up the 5-parameter astrometry solution Gaia Collaboration et al. (2023); Perryman et al. (1997), *Hipparcos* was capable of measuring parallax with milli-arcsecond precision and recorded 5-parameter astronomy solutions for 118,218 stars in the galaxy; all of the stars are available in the *Hipparcos* Catagloue by Perryman et al. (1997).

Gaia also classifies other parameters of stars such as effective temperature, metalicity and spectra. Since data release 3 (DR3) *Gaia* has mapped these parameters for over 1.8 billion sources with colour magnitudes as faint as G=21 and up to as bright as G=3 Gaia Collaboration et al. (2023).DR3 was released on 13 June 2022 and is publicly available on the *Gaia* archive, which lets users search for any star on the catalogue for free. The catalogue by Neumann et al. (2023) contains the data for all known HMXBS in the galaxy for the compact object and the optical counterpart. We use Neumann et al. (2023), also known as XRBcats, to find the optical counterpart in the *Gaia* archive. For each optical counterpart, we obtain the position, proper motions, and parallax and radial velocities (if available) to determine the peculiar velocity of each star.

1.1.1 Astrometry with GAIA

Astrometry measures a star's position, motion and distance in the sky. Stars in the galaxy are not stationary, and in the equatorial coordinate frame, they move almost linearly in the sky. Parallax measures the angular displacement of a star across the sky. As the earth rotates around the sun, the stars in the equatorial frame are displaced by the parallax angle ω this way, parallax is a measurement of distance given as:

$$d = \frac{1AU}{\omega} \tag{1.1}$$

For one arcsecond parallax, the distance is given as one parsec. Figure 1.1 is a diagram that shows how parallax and distance are measured. *Gaia* is capable of measuring the parallax of stars with milli-arcsecond precision, which scales to kilo parsec distances Gaia Collaboration et al. (2023). In *Gaia* , this is captured as the 5-parameter solution.

1. the instruments on GAIA
2. DR4 and end of mission
3. more about predecessor
4. What GAIA does better than Hipparcos
5. 5/6 parameter space

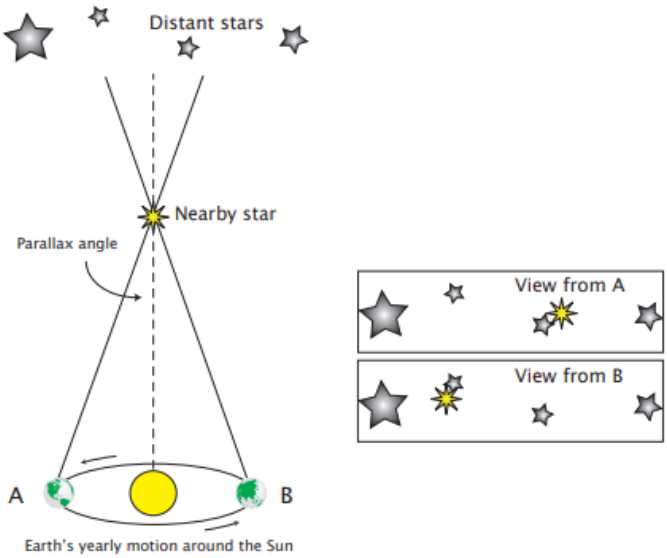

FIG. 1.1 – Model of parallax, angular displacement not to scale, Perryman (2012)

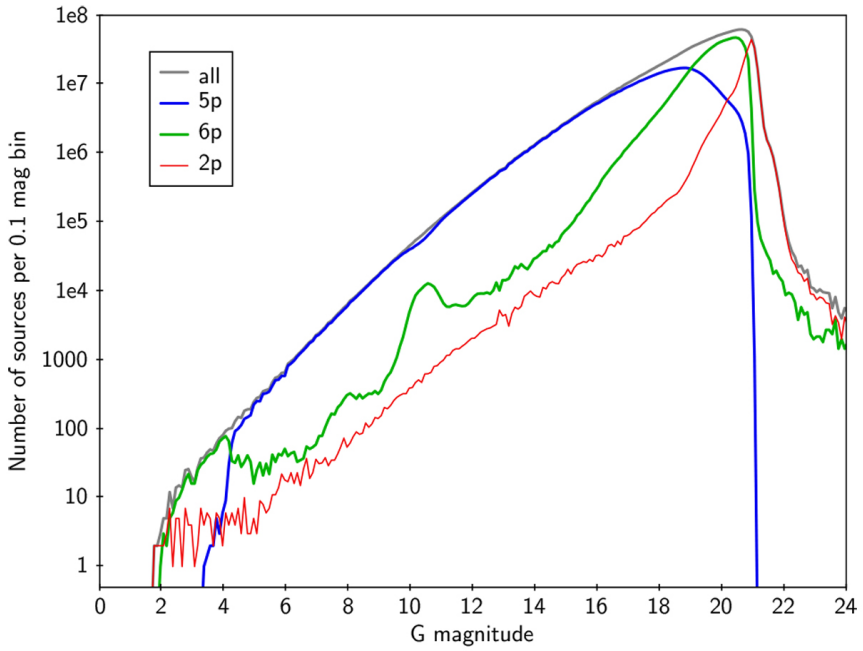

FIG. 1.2 – Quality of 5-parameter solutions with *Gaia* DR3, Lindegren et al. (2021)

1.2 Gaia's Instruments

GAIA consists of two telescopes and a focal plane. Each instrument measures flux from the common focal plane. The focal plane, comprised of 106 CCD detectors, is used to study astrometry, photometry, and radial velocity of objects that transit across the plane.

1. What is the focal plane- Absorbs the light from the
2. what are the telescopes made of
3. what is a CCD

1.2.1 Astrometric Instrument

GAIA's astrometric instrument measures the separation of stars in its field of view over an array of charge-coupled device detectors (CCD) to collect the 5-parameter or 6-parameter solution for its sources. Its wavelength band (G) covers 330nm-1150nm and can detect objects as dim as G= 21 mag Gaia Collaboration et al. (2016). The G photometric band is a broadband white light band (FIX) that measures the flux across most of the optical spectrum Gaia Collaboration et al. (2016). Sources dimmer than 21 mag may not have a full 5-parameter solution CITE GAIA EDR3. The Astrometric Instrument scans the sky continuously, measuring flux unbiased.

1.2.2 Photometric Instrument

The Photometric Instrument uses the same focal plane and telescope as the Astrometric instrument to measure the spectral energy distribution for all objects in the sky at a given epoch Gaia Collaboration et al. (2023). Light enters the instrument through two silica prisms, which separate the light into the blue photometer (BP) at 330-680 nm and the red photometer (RP) at 640-1050nm. NEED MORE INFO

1.2.3 Radial velocity Spectrometer

The *GAIA* Radial Velocity Spectrometer (RVS) offers high resolution, narrow band spectra for 33.8 million sources in the sky Gaia Collaboration et al. (2023). The RVS measures the Doppler shift of objects with its line of sight to determine the radial velocity and measure a radial velocity magnitude for the brightest stars$G_{RVS} \leq 14$. The RVS obtains the radial velocity by measuring the 845-872 nm spectra, which covers the Ca II triplet emission line. The Ca II triplet measures a star's emission

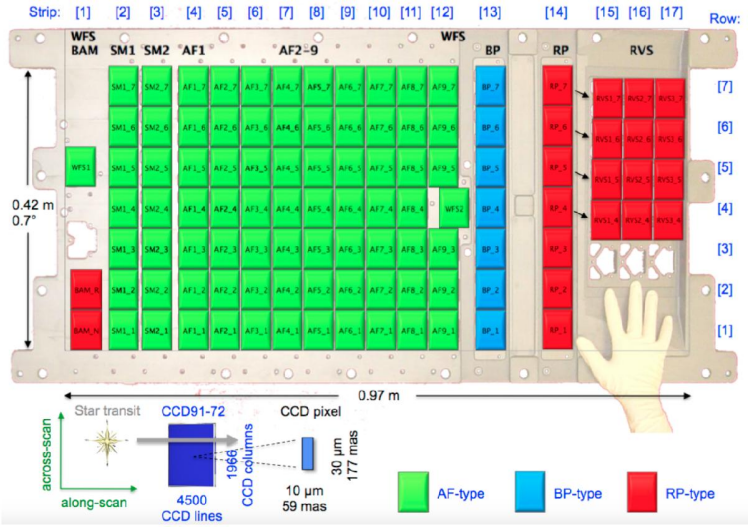

FIG. 1.3 – Schematic drawing of Focal assembly, hand for scale Gaia Collaboration et al. (2023)

spectra, metallicity, temperatures and luminosity. Gaia Collaboration et al. (2023); Sartoretti et al. (2023)

1.3 History of HMXBs

O Stars and B stars are the most massive hydrogen-burning stars in the Milky Way. Also known as population I stars, these stars are the youngest in the galaxy, which makes them essential to understanding metalicity, supernovae formation and star formation in the Milky Way. These regions are localized to the spiral arms Neumann et al. (2023). These stars were significant in determining the Oort constant for differential rotation in the galaxy Gies & Bolton (1986). Among the O and B stars, there are several stars that have significantly high space velocity and move away from their OB association; their velocity cannot be explained by redshift Gies (1987); therefore, their space velocity must come from another mechanism. In Blaauw (1961) surveyed 19 O-type and B-type stars with space velocity greater than 40km s^{-1} and classified these stars as runaways. Following the work by Blaauw (1961), further results define runaways as stars with large peculiar velocities, far distance from the galactic mid-plane or a combination of both.(Blaauw (1961); Carretero-Castrillo et al. (2023); de Wit et al. (2005)). Of the observed O-type stars in the galaxy, 30% are runways Gies (1987)

1.4 Local Standard of Rest Frame

Consider a star at point S as shown in figure 1.4. Point S is somewhere in the galactic plane, with a distance of R from the Galactic Centre. It has a 3-component velocity (Π, Θ, z), Π represents the velocity component that is positive towards the Galactic Center, $\vec{CS}$, Θ represents the positive velocity in the direction of galactic rotation, and Z represents the velocity above the midplane. The 3-component velocity represents the total velocity of the star at point S for a given time. The total velocity is comprised of 1. The star's peculiar velocity, 2. the velocity due to galactic rotation, 3.Observational bias from the sun's motion in the galaxy. If the Galactic Center rotates with velocity θ_c, then we can reduce the velocity of the star to its local standard of rest frame (LSR) as

$$\vec{V_{lsr}} = [\Pi, \Theta - \Theta_c, Z]$$

Observationally, solar motion adds systematic error to the velocity since the sun is moving in the galactic plane as well; the true LSR velocity is

$$\vec{V_{lsr}} = [\Pi - \Pi_\odot, \Theta - \Theta_c - \Theta_\odot, Z - Z_\odot]$$

Where $(\Pi_\odot, \Theta_\odot, Z_\odot)$ represent the solar motion components. The peculiar velocity is always measured with respect to the LSR frame Delhaye (1965). All stellar motion is reduced to FROM SOLAR MOTION WHEN APPLICABLE

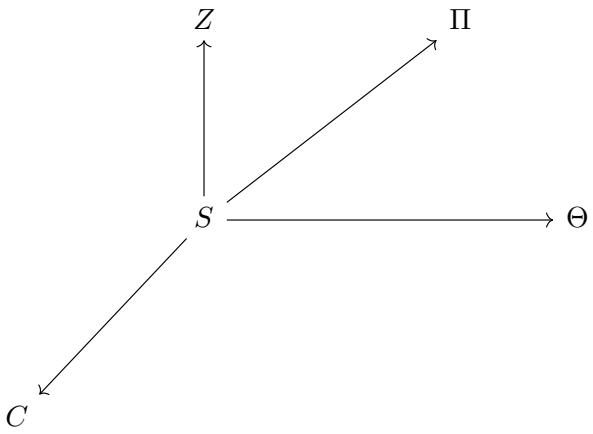

FIG. 1.4 – Local Standard of Rest Frame Delhaye (1965)

The Galactocentric distance is simply given by the law of cosine Brand & Blitz (1993), ADD A DIAGRAM Moffat et al. (1998)

1.5 Ejection Scenarios

There are two scenarios where an OB binary or Be binary can obtain a peculiar velocity. In the Supernova ejection scenario (BSS), where the supernova explosion from the most evolved star in the binary induces a high-velocity kick on the system, which ejects the binary out of its parent cluster, but the binary remains gravitationally bound, the most evolved star is now compact object Blaauw (1961); Carretero-Castrillo et al. (2023). The second scenario is the Dynamical Ejection Scenario (DES). N-body interactions in the core of a young, dense star cluster eject the binary out of the star cluster and provide a large space velocity we observe as a peculiar velocity. Carretero-Castrillo et al. (2023); Moffat et al. (1998). It is debated which ejection scenario explains the observed number of runaways in the galaxy Both models predict peculiar velocity efficiently; however, the DES seems to explain the binary frequency of runaways and some binary systems such as AE Aur and μ Col; these pairs have equal and opposite velocities with respect to their origin Gies & Bolton (1986); Moffat et al. (1998); Zinnecker & Yorke (2007). The BSS can better predict the kinematic ages and the frequency of fast rotating stars such as Be-stars Moffat et al. (1998). The BSS is much less likely when you consider that most observed runaways are single stars Gies & Bolton (1986); Gies (1987).

1. How do HMXB get peculiar velocity

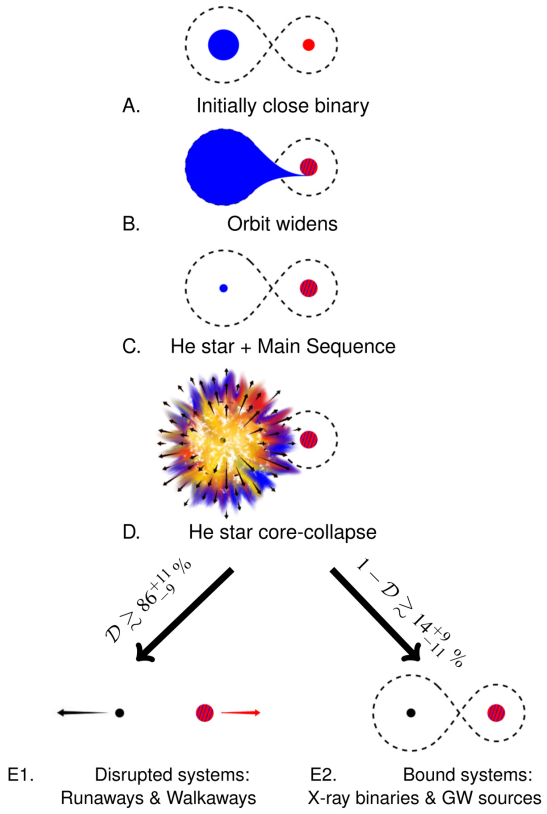

FIG. 1.5 – Cite renzo et al 2019b

2. natal kick FORTIN 2022 NS kick

1.5.1 Binary SuperNova Scenario

The compact object is a remnant of the most massive star in the progenitor system, called the primary star. As the more massive star, it evolves much faster compared to the secondary star. During the core helium burning phase of the primary, the shell expands, and the mass transfer begins onto the primary via the secondary star Blaauw (1961), Gies (1987). At the end of its lifetime, the primary star explodes into a Type II supernova, becoming a compact object. The roles are now switched; the secondary becomes the system's primary star. The system can remain bound if less than half of the total mass of the system is lost during the supernova van den Heuvel et al. (2000). The energy of the supernova creates the runaway velocity observed in HMXBs. van den Heuvel et al. (2000)

1. natal kick

2. what happens to the companions

3. van den Heuvel et al. (2000)

1.5.2 Dynamical Ejection Scenario

In the Dynamical Ejection Scenario[1], The OB binary becomes a runaway due to gravitational interactions in a young, dense star cluster. CITE POVEDA 1967 . Zinnecker and Yorke 2007. Star clusters that are young have greater gravitational encounters due to the high number density in the cluster's core which may be the reason relatively more massive stars are ejected from the cluster, Observations show the most massive stars are in the core's cluster, this means the fraction of runaways favours massive stars Phillips et al. (2024) . This is exactly described in the cluster ejection model by Gies & Bolton (1986). The OB binary interacts in a three-body interaction between other massive stars. The gravitational potential is converted into kinetic energy for the binary, and the orbital separation of the binary decreases and the binary exceeds the escape velocity of the cluster. Zinnecker & Yorke (2007)

The three-body interaction is not limited to single-binary or single-single-star interactions; binary-binary interactions become significant when the number density of stars is large or when most of the stars in the clusters are massive ($M \geq 8M_{\odot}$), Gies & Bolton (1986).

1.6 Galactic Potential of the Milky Way

Since we are interested in the motion of stars in the galaxy, some force must influence how they move. The motion of stars in the sky comes from gravity, set by the galactic potential of the Milky Way. The galactic potential is investigated by galactic rotation curve models. Typically, galactic rotation curves are studied by $H\alpha$, H-II and CO emissions lines ADD TO THIS. These models are important to determine the mass distribution of galaxies Sofue & Rubin (2001); Fich et al. (1989). More importantly, the same rotation curves allow us to predict the rotational velocity of stars around the Milky Way center independent of their distance to the center Fich et al. (1989) This is important to the stars in our catalogue as we want to compare the predicted proper motion to the proper motion observed by *Gaia* , this is what determines the peculiar velocity of each star.

Modelling the mass distribution of Galaxies is fundamental to understanding their motion. The galactic potential determines how stars orbit around the galaxy. Deriving the mass distribution

[1] Also known as Cluster Ejection Scenario.

Mass	Designation	Sp. type
8–16 $M_\odot$	Early B-type massive stars	B3V to B0V
16–32 $M_\odot$	Late O-type massive stars	O9V to O6V
32–64 $M_\odot$	Early O-type massive stars	O5V to O2V[a]
64–128 $M_\odot$	O/WR-type massive stars	WNL-H[b]

[a]O2V main-sequence stars have been identified by Walborn et al. (2002).
[b]WNL-H: N-rich late-type Wolf-Rayet (WR) stars, still on the main sequence (H-burning) (see Crowther 2007).

FIG. 1.6 – Classification of O,B and WR stars by mass Zinnecker & Yorke (2007)

1.7 O and B Binaries

O-stars and B-stars are some of the most massive main sequence stars, figure 1.6, although mass is not the only parameter that defines a star. we notice any OB stars have sufficient mass to create a type II supernova, a condition for the Binary Supernova Scenario. These stars are commonly found in OB associations, regions of loosely distributed massive stars that are important for star formations. nearly all O-stars and B-stars originated from OB associations, O-stars typically star on the main sequence for a few million years, therefore we consider OB associations as young. Blaauw (1961). Of all O-stars in the galaxy, 30% originate from OB associations and with the spiral arms of the Milky way. we are questioned as to how these binaries evolve. A possible hypothesis is mass segregation as given by Clarke & Pringle (1992). If we start with a binary in the star cluster, it is more likely to sink into the core due to gravity. Binary-Binary interactions are now more likely to occur until a stable binary system is formed, this is called a hierarchical double binary. Numerical simulations by (Clarke & Pringle, 1992) also suggest that O-stars and B-stars form binaries with similar mass stars; that is an O-stars form a binary with another O-star and similarly for B-stars. This would explain the high velocity of runaways, and the frequency of runaway binaries. About 10%-25% of runaways consist of O-stars and 2% for runaways Gies & Bolton (1986); Gies (1987)
The Popular OB associations include SCO OB1, CEP OB1 and CYG OB2, which we will explore in later sections of the thesis.

1. how we use the companions with GAIA
2. GIES AND BOLTON 1986

1.8 BeXray Binaries

Be X-Ray binaries consist of a compact object with a Be-type emission companion star. Be-stars are a subgroup of B-type stars and are quite interesting to study as they have excited Balmer lines which generates emission Abt & Cardona (1984), Boubert & Evans (2018). Their emission comes from a circumstellar disk which is formed

as a result of the rapid rotation of the Be-star around its axis Dufton et al. (2022). This circumstellar disk is also known as a deccretion disk, which is also a source of infrared emissionCarretero-Castrillo et al. (2023). Be-stars may be a product of post-mass transfer systems Pols et al. (1991) in which a B-type star transfers mass into a companion; it is suggested that this post-mass transfer produces the deccretion disk in Be-stars therefore Be-stars may be a product of binary mass transfer, although the observational fraction of Be-stars in binary is poor Pols et al. (1991). BeXray Binaries are the most common type of HMXB, and 72 of 169 candidates in XRBcats are BeXray Binaries Neumann et al. (2023).

1.9 The Compact Object

The other half of an HMXB system is the compact object. When the core of the initial supergiant stops burning, gas pressure can no longer support the star and it begins to collapse under its own gravity, After the collapse of the initial supergiant star, the remnant forms into one of three objects called the compact object; a white dwarf, a neutron star or a black hole. The white dwarf is held together by electron degeneracy pressure; therefore, its radius is inversely proportional to its mass Karttunen (1987). White dwarfs have an upper mass limit of the Chandrasekhar mass limit ($M_{ch} = 1.4M_{\odot}$). Beyond this limit, the compact object is either a neutron star or a black Orosz (2003). In Neumann et al. (2023), the compact objects are divided into X-ray sources and black hole candidates. Six of the 169 stars in XRBcats have black hole compacts, the most popular being Cygnus X-1. The low number of black hole compacts may be due to low mass loss during the supernova. The progenitor of the HMXB needs sufficient mass to become a black hole from mass transfer, the presence of a massive companion supernova already tells us there was insufficient mass to create a black hole from the progenitor.

The compact object is the source of X-ray emission, which is powered by stellar wind mass loss from the companion or by Roche lobe overflow Liu et al. (2006); Blaauw (1961).

1.10 Galactic Rotation Model

Galactic rotation curves are fundamental to understanding the mass distribution of galaxies. These curves explain the rotational velocity of stars in the galaxy as a function of distance to the galactic centre. Rotation curves are calculated by various methods,a common method is the Tangent-point method, which measures the emission lines of HI and CO molecules Fich et al. (1989). The tangent-point method measures the terminal velocity of HI and CO around quadrants of the galaxy. The terminal velocity is converted into a rotational velocity; we follow Fich et al. (1989),

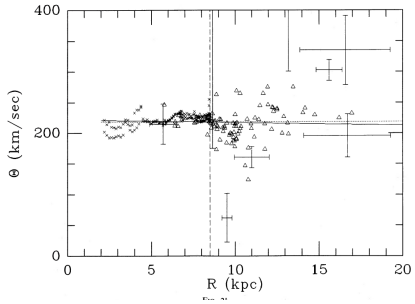

FIG. 1.7 – HI tangent point data, CO in triangles, with best-fit rotation curve lines for a linear and power-law fit. from Fich et al. (1989). dashed line represents solar value R_o, Θ_o = (8.5kpc,220km/s)

which determines the rotational velocity of molecules and their distance from the galactic centre. Table 2 in Fich et al. (1989) provides the rotational velocity for various galactic longitude regions at b=0°. The data from the tangent-point method is fit to a curve that determines the circular velocity of an object from its distance from the galactic centre. That is, we can assign a circular velocity for any star if we know its distance to the galactic centre.

Figure Fich et al. (1989) shows HI tangent points used to measure the rotation curve for Galactic distance, 3kpc to 17kpc from the galactic centre. The solar radius $R_o = 8.5kpc$ is the sun's distance to the galactic centre and solar circular velocity ($\Theta = 220km/s$) represents the circular orbit velocity of a sun around the galaxy.

The best-fit model to the data is a power law given as:

$$\theta(R) = \theta_o(a_1 \frac{R}{R_o}^{a_2} + a_3) \tag{1.2}$$

Where a_1, a_2, a_3 are constants selected such that $\Theta(R = R_o) = \Theta_o$. R is the galactocentric distance given by the law of cosine as

$$R = \left(R_0^2 + d^2 - 2R_0 d\cos l\right)^{1/2} \tag{1.3}$$

For a flat rotation curve model, the angular speed $\omega = \frac{\Theta}{R}$ limits the distance of stars examined. Stars close to the sun have small circular velocities; any non-circular velocity will significantly exaggerate ω and contribute to large error; therefore, nearby stars are omitted from the fit Fich et al. (1989). We use the angular speed to determine the galactic rotation velocity of a star with respect to its local standard of rest (see 1.4). This model is valid for stars within $2R_o$.

1. SOFUE 2014 AND FICH 1989
2. Limitations
3. old model and update with OOrt FUNDAMENTAL ASTRONOMY BOOK
4. application to HMXB and peculiar velocity
5. should move LSR section to before or after this

1.11 Traceback Path of Stars

1.12 Membership Analysis

Later, after we select targets from the traceback path, can do this end of Feburary

Chapter 2

Chapter 2 - Data Selection and Analysis

2.1 XRBCats Catalogue

Neumann et al. (2023) based off of Liu et al. (2006)

ADD CROSS MATCH WITH FORITN ET AL Fortin et al. (2023) NAME, MASS COMPACT MASS COMPANION

2.1.1 Limitations of Parallax

LOOK AT APELLANIZ 2022 AN ESTIMATION OF THE GAIA EDR3 PARALLAX BIAS

2.2 Query with *Gaia*

Gaia DR3 is stored for free and public use on the Gaia archive. The archive includes 5-parameter solutions for over 1.8 billion sources plus photometric measurements. The data is easily accessible using Astronomical Data Query Language (ADQL), an astronomy subset of SQL Gaia Collaboration et al. (2023). The catalogue from Neumann et al. (2023) contains *Gaia* source identifiers for 121 stars. For each star with a source identifier, the 5-parameter solutions are collected along with the radial velocity, G band magnitude and respective errors. The data is collected into .csv and .ecsv files.

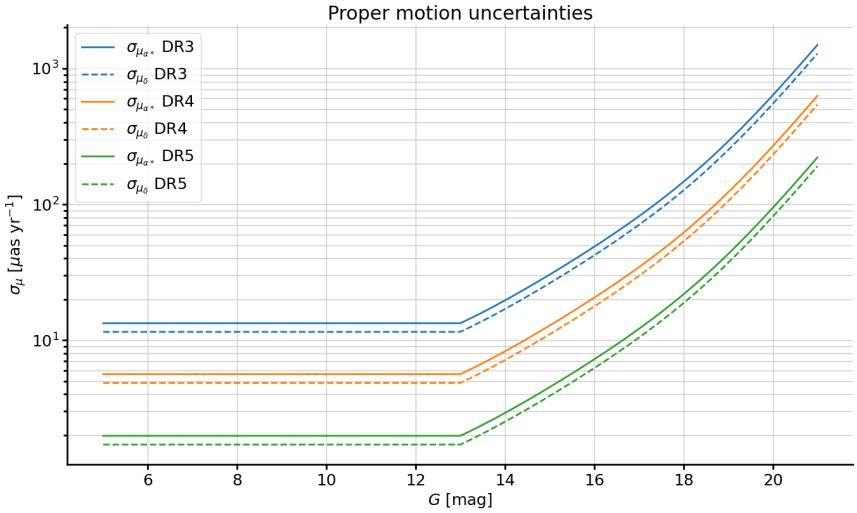

FIG. 2.1 – Gaia Proper motion uncertainty source

2.3 Proper Motion of Stars

Moffat et al. (1998),

TRANSFORMATION BY POLESKI

2.4 Galactic Rotation

and galactocentric distance, Fich et al. (1989); Moffat et al. (1998)

2.5 Peculiar Velocity

The peculiar velocity is simply the difference between the observed motion of a star and its expected motion. In terms of proper motion μ, the total 2D proper motion is the sum of the galactic rotation (μ_{rot}), the solar proper motion ($\mu_\odot$) and the peculiar motion (μ_{pec}). The solar motion represents a star's motion with respect to the sun Moffat et al. (1998).

$$\begin{aligned} \mu_l &= (\mu_l)_\odot + (\mu_l)_{rot} + (\mu_l)_{pec} \\ \mu_b &= (\mu_b)_\odot + (\mu_b)_{rot} + (\mu_b)_{pec} \end{aligned} \tag{2.1}$$

The observed proper motion for each star is observed by *Gaia* and the rotation model for a flat rotational curve is given by the galactic potential Fich et al. (1989), which

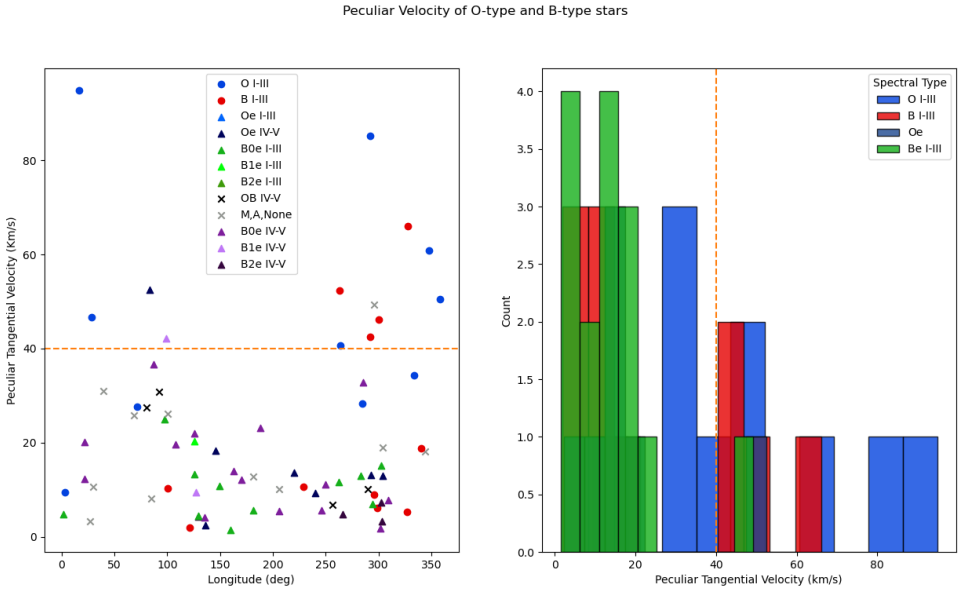

FIG. 2.2 – Peculiar velocity

is accurate up to $2R_o$, each star is corrected for solar motion by
INSERT SOLAR MOTION EQUATION
What is left is the peculiar motion of the optical counterpart, which describes the degree to which a binary is a runaway system.

$$v_{pec} = K * d * \sqrt{(\mu_l)^2_{pec} + (\mu_b)^2_{pec}} \tag{2.2}$$

Equation 2.1 converts peculiar motion to velocity in kilometres per second.

Chapter 3

Chapter 3 - Results

3.1 Galactic Traceback

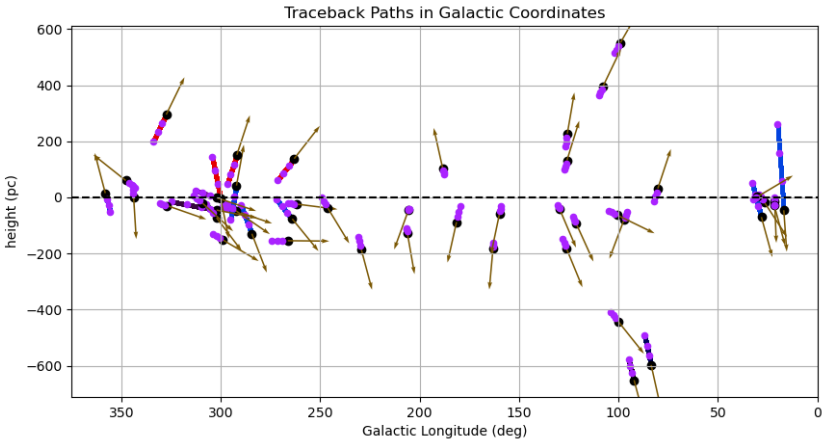

FIG. 3.1 – Galactic path for stars leaving the galactic midplane

Chapter 4

Acknowledgements

This work has made use of data from the European Space Agency (ESA) mission *Gaia* (https://www.cosmos.esa.int/gaia), processed by the *Gaia* Data Processing and Analysis Consortium (DPAC, https://www.cosmos.esa.int/web/gaia/dpac/consortium). Funding for the DPAC has been provided by national institutions, in particular the institutions participating in the *Gaia* Multilateral Agreement.

4.1

Name	SpType	G	l	b	Parallax	distance	μ_l cos(b)	μ_b	$Vpec$	Mx
		mag	deg	deg	mas	kpc	mas/yr	mas/yr	km/s	$M_\odot$
1A 0535+262	O9.7IIIe	8.60	181.44	-2.64	0.53(0.0230)	1.91(0.0850)	2.13	-2.03	12.76	NaN
1A 1118-61	O9.5Ve	11.59	292.50	-0.89	0.33(0.0110)	3.04(0.1060)	-5.57	-0.51	13.18	NaN
1E 1145.1-6141	B2Iae	12.26	295.49	-0.01	0.13(0.0100)	7.89(0.6380)	-6.61	0.83	49.26	1.70
1ES 1210-64.6	B5V	13.98	298.89	-2.30	0.26(0.0180)	3.78(0.2530)	-5.96	-0.38	6.14	NaN
1FGL J1018.6-5856	O6V((f))	12.27	284.35	-1.69	0.23(0.0100)	4.40(0.1980)	-6.65	-1.59	28.33	2.00
1H 2202+501	B3e	9.30	97.25	-4.04	0.88(0.0130)	1.14(0.0170)	1.73	-1.64	24.95	NaN
2S 0114+650	B1Iae	10.52	125.71	2.56	0.20(0.0110)	5.09(0.2920)	-1.32	0.62	20.31	NaN
3U 1223-62	B1 Ia+	9.75	300.10	-0.04	0.25(0.0160)	3.99(0.2550)	-5.03	-2.52	46.23	NaN
3U 1258-61	B2 Vne	12.65	304.10	1.25	0.54(0.0140)	1.85(0.0480)	-4.35	-0.03	18.95	NaN
4U 0115+63	B0.2Ve	14.30	125.92	1.03	0.14(0.0160)	7.34(0.8800)	-1.73	0.31	21.92	NaN
4U 0352+309	B0Ve	6.26	163.08	-17.14	1.63(0.0370)	0.61(0.0140)	0.31	-2.25	14.03	NaN
4U 0728-25	O5Ve	11.60	240.28	-4.05	0.10(0.0170)	10.44(1.8650)	-1.99	0.09	9.27	NaN
4U 1145-619	B0.2 III	8.65	295.61	-0.24	0.47(0.0170)	2.10(0.0770)	-6.43	0.10	8.98	NaN
4U 1538-52	B0 Iab	13.16	327.42	2.16	0.13(0.0150)	7.82(0.9320)	-7.83	0.83	66.08	NaN
4U 1954+31	M4 I	8.36	68.39	1.93	0.26(0.0240)	3.88(0.3690)	-6.30	-1.35	25.84	NaN
4U 2206+54	O9.5IIIe	9.74	100.60	-1.11	0.30(0.0140)	3.28(0.1460)	-5.32	-0.32	26.16	NaN
AX J1700.2-4220	B2e	8.71	343.80	-0.03	0.64(0.0230)	1.56(0.0560)	-0.44	-1.83	18.07	NaN
AX J1845.0-0433	O9.5I	12.76	28.14	-0.66	0.16(0.0240)	6.10(0.8810)	-5.60	-1.36	46.70	NaN
BSD 24-491	B0e	10.40	159.85	-1.27	0.38(0.0150)	2.64(0.1050)	0.96	-0.70	1.44	NaN
CCDM J07474-5320A	B7 IV-Ve	7.54	266.31	-13.73	1.54(0.0210)	0.65(0.0090)	-9.68	-0.06	4.80	NaN
Cen X-3	O6.5 II-III	12.88	292.09	0.34	0.14(0.0140)	7.21(0.7120)	-3.72	1.16	85.15	1.34
Cep X-4	B1-B2Ve	13.82	99.01	3.31	0.10(0.0130)	9.54(1.1520)	-3.68	0.27	42.12	NaN
Cyg X-1	O9.7Iabpvar	8.54	71.33	3.07	0.44(0.0150)	2.25(0.0760)	-7.37	-0.10	27.64	21.20
GRO J1008-57	B0 IIIVe	13.88	283.00	-1.82	0.24(0.0130)	4.12(0.2240)	-5.89	0.25	13.02	NaN
GRO J2058+42	O9.5-B0IV-Ve	14.13	83.57	-2.65	0.08(0.0150)	12.90(2.5350)	-3.98	-0.56	52.48	NaN
Ginga 0834-430	B0-2III-Ve	19.15	262.02	-1.51	1.10(0.2170)	0.91(0.1780)	-4.95	-0.28	11.55	NaN

HD 110432	B0.5IVpe	5.14	301.96	-0.20	2.28(0.0770)	0.44(0.0150)	-12.77	-3.98	1.78	NaN
HD 119682	B0Ve	8.52	309.15	-0.72	0.60(0.0290)	1.65(0.0780)	-5.13	-1.16	7.78	NaN
HD 141926	B2 IIIn	8.69	326.98	-1.24	0.73(0.0180)	1.37(0.0340)	-4.46	-0.46	5.22	NaN
HD 153919	O6Iafcp	6.42	347.75	2.17	0.63(0.0260)	1.58(0.0650)	5.46	1.11	60.92	NaN
HD 161103	B0.5 III-Ve	8.23	1.36	1.05	0.79(0.0240)	1.27(0.0380)	-2.41	-0.47	4.74	NaN
HD 215227	B1.5-B2III	8.71	100.17	-12.40	0.49(0.0180)	2.06(0.0780)	-4.56	-1.13	10.30	NaN
HD 249179	B5ne	10.01	181.28	1.86	0.60(0.0300)	1.67(0.0840)	2.21	-0.55	5.54	NaN
HD 34921	B0 IVpe	7.23	170.05	0.71	0.72(0.0300)	1.39(0.0580)	4.04	-1.18	12.13	NaN
HD 77581	B0.5 Ib	6.74	263.06	3.93	0.50(0.0150)	2.02(0.0620)	-10.13	2.61	52.43	NaN
HD 96670	O8.5f(n)p	7.35	290.20	0.40	0.31(0.0280)	3.22(0.2910)	-6.88	-1.01	10.09	6.20
HESS J0632+057	B0Vpe	8.88	205.67	-1.44	0.54(0.0230)	1.85(0.0780)	0.37	-0.22	5.47	NaN
HR 4804	B8Vn(e)	6.54	302.14	-12.52	4.77(0.0270)	0.21(0.0010)	-26.97	-9.99	7.20	NaN
IGR J00370+6122	BN0.5II-III / BN0.7Ib	9.46	121.22	-1.46	0.27(0.0120)	3.68(0.1630)	-1.82	-0.44	1.92	NaN
IGR J01363+6610	B1Ve	12.46	127.39	3.73	0.17(0.0110)	5.99(0.3940)	-1.59	-0.32	9.42	NaN
IGR J01583+6713	B2IVe	13.69	129.35	5.19	0.13(0.0130)	7.50(0.7400)	-1.24	-0.03	4.25	NaN
IGR J06074+2205	B0.5Ve	12.17	188.38	0.81	0.14(0.0180)	7.24(0.9470)	0.81	0.20	23.13	NaN
IGR J08262-3736	OBV	12.16	256.44	0.28	0.18(0.0100)	5.63(0.3060)	-3.96	-0.05	6.70	NaN
IGR J08408-4503	O8.5Ib-II(f)p	7.45	264.04	-1.95	0.44(0.0170)	2.26(0.0860)	-9.41	-2.08	40.72	NaN
IGR J11215-5952	B0.5Ia	9.77	291.89	1.07	0.12(0.0120)	8.11(0.8110)	-5.76	0.88	42.47	NaN
IGR J11305-6256	B0IIIne	8.13	293.94	-1.49	0.57(0.0470)	1.75(0.1420)	-6.23	-0.49	7.02	NaN
IGR J16195-4945	ON9.7Iab	16.37	333.56	0.34	0.36(0.0510)	2.79(0.3920)	-0.52	-0.26	34.32	NaN
IGR J16465-4507	B0.5-1Ib	13.48	340.05	0.14	0.30(0.0170)	3.38(0.1970)	-3.48	-0.63	18.82	NaN
IGR J17544-2619	O9Ib	11.66	3.24	-0.34	0.40(0.0270)	2.52(0.1700)	-0.83	0.10	9.44	1.40
IGR J18406-0539	B5V	11.23	26.66	-0.23	0.23(0.0150)	4.30(0.2690)	-3.08	-0.45	3.22	NaN
IGR J18462-0223	NaN	17.65	30.22	0.08	0.68(0.1210)	1.48(0.2640)	-2.65	0.43	10.63	NaN
IGR J21343+4738	B1–1.5III–V	14.00	92.17	-3.12	0.08(0.0140)	11.97(2.0300)	-3.35	-0.43	30.81	NaN
LS 1698	B0V-IIIe	11.24	285.35	1.43	0.17(0.0160)	5.84(0.5540)	-6.97	-0.40	32.74	NaN
LS 5039	ON6V((f))z	10.80	16.88	-1.29	0.49(0.0150)	2.04(0.0630)	-3.73	-10.38	94.91	NaN
LS 992	B0.2IVe	12.42	249.58	1.54	0.12(0.0120)	8.45(0.8750)	-2.59	-0.01	11.06	NaN

LS I +61 303	B0Ve	10.40	135.68	1.09	0.38(0.0130)	2.65(0.0910)	-0.28	-0.41	4.17	NaN
MAXI J0709-159	NaN	9.19	229.31	-3.36	0.32(0.0240)	3.17(0.2440)	-2.06	-0.99	10.59	NaN
MXB 0656-072	O9.7Ve	11.98	220.13	-1.77	0.15(0.0150)	6.50(0.6400)	-1.41	0.01	13.58	NaN
NGC 6649 9	B0Ve	10.96	21.64	-0.79	0.47(0.0280)	2.11(0.1250)	-0.09	-0.06	20.05	NaN
PSR B1259-63	O9.5Ve	9.63	304.18	-0.99	0.44(0.0130)	2.25(0.0680)	-7.10	0.04	12.99	NaN
PSR J0635+0533	B1IIIe-B2Ve	12.50	206.15	-1.04	0.14(0.0150)	7.02(0.7350)	-0.55	-0.18	10.19	NaN
PSR J2032+4127	B0:e/B0:Vn	11.28	80.22	1.03	0.57(0.0160)	1.76(0.0480)	-2.49	1.73	27.43	NaN
RX J0146.9+6121	B1III-Ve	11.21	129.54	-0.80	0.33(0.0220)	3.05(0.2010)	-0.99	-0.31	4.52	NaN
SAO 49725	B0.5III-Ve	9.03	85.23	5.05	0.42(0.0160)	2.38(0.0910)	-5.26	-0.51	8.06	NaN
SAX J2103.5+4545	B0Ve	13.77	87.13	-0.69	0.13(0.0130)	7.64(0.7560)	-4.70	0.46	36.70	NaN
SAX J2239.3+6116	B0Ve	14.11	107.73	2.36	0.10(0.0140)	9.62(1.2920)	-2.54	0.22	19.68	NaN
SGR 0755-2933	B0Ve	9.94	246.23	-0.61	0.28(0.0140)	3.50(0.1710)	-3.86	-0.73	5.56	1.40
SRGA J124404.1-632232	Be	15.08	302.11	-0.52	0.12(0.0220)	8.11(1.4580)	-6.35	-0.42	15.15	NaN
SS 397	B0.5Ve	11.72	21.47	-0.87	1.08(0.1940)	0.93(0.1670)	-0.10	-1.11	12.36	NaN
SS 433	A3-7 I	12.60	39.69	-2.25	0.12(0.0230)	8.46(1.6660)	-5.64	0.45	31.01	4.20
Swift J0243.6+6124	O9.5Ve	12.39	135.93	1.43	0.18(0.0110)	5.51(0.3440)	-0.72	-0.19	2.38	NaN
TYC 3681-695-1	B1-2 III/Ve	11.41	126.08	-3.57	0.34(0.0180)	2.95(0.1570)	-2.39	-0.80	13.26	NaN
V0332+53	O8-9Ve	14.20	146.05	-2.19	0.13(0.0200)	7.44(1.1160)	-0.48	0.20	18.23	NaN
XTE J0421+560	B1/2I[e]	10.77	149.18	4.13	0.21(0.0150)	4.76(0.3370)	0.03	-0.69	10.76	NaN
XTE J1739-302	O8Iab(f)	12.64	358.07	0.45	0.52(0.0480)	1.94(0.1800)	2.96	2.36	50.50	NaN
mu.02 Cru	B5Vne	5.15	303.37	5.70	8.27(0.1170)	0.12(0.0020)	-28.61	-9.82	3.28	NaN

Bibliography

Abt H. A., Cardona O., 1984, The Astrophysical Journal, 285, 190

Blaauw A., 1961, Bulletin Astronomical Institute of the Netherlands, 15, 265

Boubert D., Evans N. W., 2018, Monthly Notices of the RAS, 477, 5261

Brand J., Blitz L., 1993, Astronomy and Astrophysics, 275, 67

Carretero-Castrillo M., Ribó M., Paredes J. M., 2023, Astronomy and Astrophysics, 679, A109

Chevalier C., Ilovaisky S. A., 1998, Astronomy and Astrophysics, 330, 201

Clarke C. J., Pringle J. E., 1992, Monthly Notices of the Royal Astronomical Society, 255, 423

Delhaye J., 1965, in Blaauw A., Schmidt M., eds, , Galactic structure. Edited by Adriaan Blaauw and Maarten Schmidt.. University of Chicago Press, p. 61

Dufton P. L., Lennon D. J., Villaseñor J. I., Howarth I. D., Evans C. J., de Mink S. E., Sana H., Taylor W. D., 2022, Monthly Notices of the RAS, 512, 3331

Fich M., Blitz L., Stark A. A., 1989, The Astrophysical Journal, 342, 272

Fortin F., García F., Simaz Bunzel A., Chaty S., 2023, Astronomy and Astrophysics, 671, A149

Gaia Collaboration et al., 2016, Astronomy and Astrophysics, 595, A1

Gaia Collaboration et al., 2023, Astronomy and Astrophysics, 674, A1

Gies D. R., 1987, Astrophysical Journal, Supplement, 64, 545

Gies D. R., Bolton C. T., 1986, Astrophysical Journal, Supplement, 61, 419

Karttunen H., 1987, Fundamental astronomy. Springer

Lindegren L., et al., 2021, Astronomy and Astrophysics, 649, A2

Liu Q. Z., van Paradijs J., van den Heuvel E. P. J., 2006, Astronomy and Astrophysics, 455, 1165

Maíz Apellániz J., Pantaleoni González M., Barbá R. H., Simón-Díaz S., Negueruela I., Lennon D. J., Sota A., Trigueros Páez E., 2018, Astronomy and Astrophysics, 616, A149

Moffat A. F. J., et al., 1998, Astronomy and Astrophysics, 331, 949

Neumann M., Avakyan A., Doroshenko V., Santangelo A., 2023, Astronomy and Astrophysics, 677, A134

Orosz J. A., 2003, in van der Hucht K., Herrero A., Esteban C., eds, IAU Symposium Vol. 212, A Massive Star Odyssey: From Main Sequence to Supernova. p. 365 (arXiv:astro-ph/0209041), doi:10.48550/arXiv.astro-ph/0209041

Perryman M., 2012, European Physical Journal H, 37, 745

Perryman M. A. C., et al., 1997, Astronomy and Astrophysics, 323, L49

Phillips G. D., Oey M. S., Cuevas M., Castro N., Kothari R., 2024, The Astrophysical Journal, 966, 243

Pols O. R., Cote J., Waters L. B. F. M., Heise J., 1991, Astronomy and Astrophysics, 241, 419

Sartoretti P., et al., 2023, Astronomy and Astrophysics, 674, A6

Sofue Y., Rubin V., 2001, Annual Review of Astronomy and Astrophysics, 39, 137–174

Zinnecker H., Yorke H. W., 2007, Annual Review of Astron and Astrophysics, 45, 481

de Wit W. J., Testi L., Palla F., Zinnecker H., 2005, Astronomy and Astrophysics, 437, 247

van den Heuvel E. P. J., Portegies Zwart S. F., Bhattacharya D., Kaper L., 2000, Astronomy and Astrophysics, 364, 563